JCTC Journal of Chemical Theory and Computation

Article

pubs.acs.org/JCTC

Multiconfiguration Pair-Density Functional Theory: A Fully Translated Gradient Approximation and Its Performance for Transition Metal Dimers and the Spectroscopy of $Re_2Cl_8^{2-}$

Rebecca K. Carlson, Donald G. Truhlar,* and Laura Gagliardi*

Department of Chemistry, Chemical Theory Center, and Supercomputing Institute, University of Minnesota, Minneapolis, Minnesota 55455, United States

Supporting Information

ABSTRACT: We extend the on-top density functional of multiconfiguration pair-density functional theory (MC-PDFT) to include the gradient of the on-top density as well as the gradient of the density. We find that the theory is reasonably stable to this extension; furthermore, it provides improved accuracy for molecules containing transition metals. We illustrate the extended on-top density functionals by applying them to Cr_2, Cu_2, Ag_2, Os_2, and $Re_2Cl_8^{2-}$ as well as to our previous database of 56 data for bond dissociation energies, barrier heights, reaction energies, proton affinities, and the water dimer. The performance of MC-PDFT is comparable to or better than that of CASPT2.

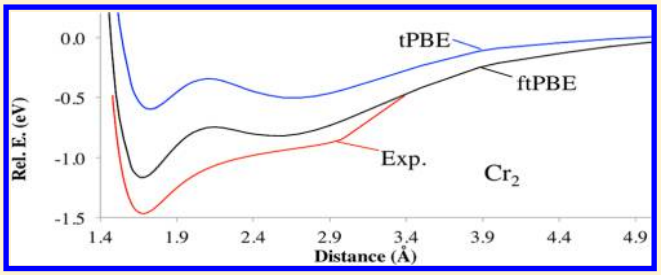

1. INTRODUCTION

Properly describing the dissociation of diatomic molecules can be problematic for both wave function theory (WFT) and Kohn−Sham density functional theory (KS-DFT).[1] To keep the spin and space symmetry of even simple dissociating diatomics such as H_2 or N_2, a multideterminant wave function is necessary; for a single determinant, symmetry breaking is needed.[2−5] In Kohn−Sham theory, a broken-symmetry solution may yield accurate energetics at the equilibrium geometry and dissociation limit, but a Slater determinant of the noninteracting reference system is nonphysical at the dissociation limit.[6,7] If the exact exchange-correlation functional were known, then the single Slater determinant obtained by minimizing its energy would yield correct energetics despite the inherently multideterminantal character of dissociation.[1,8] However, currently available density functionals are limited in their ability to model systems with intrinsically multideterminantal character[9−12] (such systems are called multireference systems or systems with high static correlation). When the symmetry of the Slater determinant is severely broken, the state being modeled may be ambiguous.

Transition metal dimers with a high level of multireference character are also challenging for WFT. For example, the ground state of Cr_2 is a $^1\Sigma_g^+$ state, where, at the equilibrium geometry, there is a formal bond order of six;[13] the molecule dissociates to atoms in the ^{7}S configuration, coupled to make an overall spin singlet. There is significant multireference character such that the Hartree−Fock configuration is only about 47% of the wave function at equilibrium.[14] The most accurate WFT potential energy curves for the Cr_2 system have been obtained using complete active space self-consistent field[15] (CASSCF) theory, followed by a complete active space second order perturbation[16] (CASPT2) or the split generalized active space[17] (SplitGAS) methods. Such calculations, like the one by Ruipérez et al.[14] that uses a molecule-specific ionization potential-electron affinity (IPEA) shift (an empirical parameter introduced in the zeroth-order Hamiltonian in the CASPT2 method), can yield a potential energy curve that mimics the features of the experimental curve,[13] i.e., a minimum around 1.678 Å and a shoulder around 2.6 Å, but those CASPT2 calculations overestimate the dissociation energy, which should be around 1.47 eV.[14,17] When one uses the standard value for the empirical IPEA shift, the results are worse. Coupled cluster theory needs higher than the connected triple excitations of the so-called gold standard CCSD(T) method to accurately reproduce experiment, and this makes the cost prohibitively expensive for typical Cr-containing molecules.[18] For KS-DFT, the bond length and dissociation energy of Cr_2 may be overestimated or underestimated, depending on the functional.[19−22]

Not only are transition metal dimers with a large amount of static correlation a challenge for quantum chemistry, but challenges are also presented by those dimers for which dynamic correlation dominates at equilibrium. For Cu_2 and Ag_2, there is a single bond between the atoms of the 4s or 5s σ_g orbitals, respectively, with the 3d subshell (for Cu_2) and the 4d subshell (for Ag_2) being completely full. Both molecules have a $^1\Sigma_g^+$ ground state and dissociate to atoms in the ^{2}S configuration. As with Cr_2, depending on the choice of the exchange-correlation functional and basis set, KS-DFT may predict the correct geometry or dissociation energy, but it will not predict both.[19−21,23] For Cu_2, CASPT2 has been found to reproduce the experimental geometry but to underestimate the dissociation

Received: April 25, 2015
Published: July 24, 2015

DOI: 10.1021/acs.jctc.5b00609
J. Chem. Theory Comput. 2015, 11, 4077−4085

energy by 0.01 to 0.24 eV, depending on the basis set, relativistic corrections, and type of Fock matrix employed in the calculation.[24]

We have recently presented a new form of density functional theory, namely, multiconfiguration pair-density functional theory (MC-PDFT), a post-SCF method (in the current implementation) that is able to treat intrinsically multideterminantal systems in a physical way.[25,26] MC-PDFT combines multiconfigurational self-consistent field (MCSCF) wave functions with a new kind of density functional called the on-top density functional to distinguish it from the exchange-correlation functional of KS-DFT. The MCSCF wave function is used to compute kinetic energy and classical Coulomb contributions to the electronic energy as well as the total density ρ, on-top pair density Π, and their gradients, which are variables in the on-top density functional that is used to compute the remaining contributions to the energy. KS-DFT involves only the one-particle density, as justified by the Hohenberg–Kohn theorem,[8] but MC-PDFT goes beyond that as the on-top pair density is a two-particle quantity. MC-PDFT can treat intrinsically multideterminantal systems with the correct spin and space symmetry, and it approximates the sum of the static and dynamic correlation energies without attempting to separate them. The use of the on-top density as an ingredient in combining multiconfigurational WFT with DFT is not new (see previous discussions and methods[27−29]), but the present approach of calculating the correlation energy from the on-top density, without using the CASSCF wave function to estimate the correlation energy, avoids the double counting of the portion of the correlation energy that is contained in the MCSCF energy estimate. This double counting problem has been one of the chief drawbacks of previous attempts to combine density functional theory with a multideterminantal representation of the density.

In previous work, we obtained first approximations to the on-top density functional by a translation prescription starting with the local-spin-density approximation or a gradient approximation (GA) to the exchange-correlation functionals. For example, we obtained the translated PBE functional, called tPBE, by translating the PBE[28] exchange-correlation functional. In the translation prescription, we did not translate the gradient of the on-top density. The first goal of the present article is to show that we can include the gradient of the on-top density (resulting in a functional we call fully translated PBE or ftPBE) in a stable way, and we illustrate the fully translated functional by results on the CE56 database that we presented in a previous article.[26] The second goal of the present article is to present calculated potential energy curves for Cr_2, Cu_2, Ag_2, and Os_2 and the well-known $\delta-\delta^*$ excitation in $Re_2Cl_8^{2-}$ with MC-PDFT using both the tPBE and ftPBE functionals.

We will start with a concise review of multiconfiguration pair-density functional theory, and we will then describe the new functional.

2. MULTICONFIGURATION PAIR-DENSITY FUNCTIONAL THEORY

Using a nonrelativistic, Born–Oppenheimer Hamiltonian, the usual energy expression for a multiconfiguration electronic wave function is given by

$$E = V_{nn} + \sum_{pq} h_{pq}D_{pq} + \frac{1}{2}\sum_{pqrs} g_{pqrs}d_{pqrs} \tag{1}$$

where V_{nn} is the sum of nuclear–nuclear repulsion terms, h_{pq} and g_{pqrs} are the one- and two-electron integrals, respectively, and D_{pq} and d_{pqrs} are the one- and two-body electronic density matrices, respectively. Indices p, q, r, and s refer to generic orbitals. By distinguishing between inactive orbitals (doubly occupied in all configurations generated by the CASSCF wave function, indices i and j) and active orbitals (indices v, w, x, and y), the energy expression for a CASSCF wave function becomes

$$E = V_{nn} + 2\sum_{i} h_{ii} + \sum_{ij}(2g_{iijj} - g_{ijij}) + \sum_{vw} h_{vw}D_{vw} + \sum_{ivw}(2g_{iivw} - g_{iviw})D_{vw} + \frac{1}{2}\sum_{vwxy} g_{vwxy}d_{vwxy} \tag{2}$$

In MC-PDFT energy, we replace eq 2 by

$$E = V_{nn} + 2\sum_{i} h_{ii} + 2\sum_{ij} g_{iijj} + \sum_{vw} h_{vw}D_{vw} + 2\sum_{ivw} g_{iivw}D_{vw} + \frac{1}{2}\sum_{vwxy} g_{vwxy}D_{vw}D_{xy} + E_{ot}[\rho,\Pi] \tag{3}$$

where $E_{ot}[\rho,\Pi]$ is the on-top density functional of the total density ρ and on-top pair density Π. The difference between eq 2 and eq 3 is in that the two-electron contribution has been replaced by a Coulomb term involving the product of one-body density matrices and a functional of the total density and on-top density.

3. TRANSLATED AND FULLY TRANSLATED FUNCTIONALS

A gradient approximation to the exchange-correlation energy can be written in terms of the total density ρ, the spin magnetization density m, and their gradients, where

$$\rho(\mathbf{r}) = \rho_\alpha(\mathbf{r}) + \rho_\beta(\mathbf{r}) \tag{4}$$

and

$$m(\mathbf{r}) = \rho_\alpha(\mathbf{r}) - \rho_\beta(\mathbf{r}) \tag{5}$$

and where ρ_α is the density of spin-up electrons and ρ_β is the density of spin-down electrons at a point $\mathbf{r}$. We then write the functional dependence of a gradient approximation as

$$E_{xc} = E_{xc}(\rho,m,\rho',m') \tag{6a}$$

where

$$\rho' = \nabla\rho \tag{6b}$$

$$m' = \nabla m \tag{6c}$$

To enable the treatment of open-shell states with a proper representation of the symmetry, the spin-free quantities ρ and Π, are used, where Π is the on-top pair density defined by[29]

$$\Pi(\mathbf{r}) = \binom{N}{2}\int |\Psi(x_1,x_2,\ldots,x_N)|^2 d\sigma_1 d\sigma_2 \ldots d\sigma_N d\mathbf{r}_3 d\mathbf{r}_4 \ldots d\mathbf{r}_N|_{\mathbf{r}_1=\mathbf{r}_2=\mathbf{r}} \tag{7a}$$

In eq 7a, N is the number of electrons, Ψ is the wave function, and x_i denotes the spatial ($\mathbf{r}_i$) and spin (σ_i) coordinates of electron i. Note that our definition of Π differs from that in ref 29 by a factor of 2 (we use the definition of ref 27i). If a wave function is a single Slater determinant, then one can show that[29]

$$m(\mathbf{r}) = \rho(\mathbf{r})\chi(R(\mathbf{r})) \tag{7b}$$

DOI: 10.1021/acs.jctc.5b00609
J. Chem. Theory Comput. 2015, 11, 4077−4085

where

$$\chi(R) = [1 - R]^{1/2} \tag{7c}$$

and

$$R(\mathbf{r}) = \frac{4\Pi(\mathbf{r})}{[\rho(\mathbf{r})]^2} \tag{7d}$$

For a single Slater determinant, $R \leq 1$ at all points in space. However, for wave functions that are multiconfigurational, eq 7b is not true, and R can be larger than unity.[29]

In MC-PDFT, we use ρ and Π to define the on-top density functional. Although, eventually, new on-top functionals should be developed directly in terms of ρ and Π, in our work so far we obtain the on-top functional by translating existing exchange-correlation functionals. In our original translation,[25] we used the following prescription for translation

$$E_{ot}[\rho(\mathbf{r}),\Pi(\mathbf{r})] = E_{xc}\left(\rho(\mathbf{r}),\begin{cases}\rho(\mathbf{r})(1-R)^{1/2} \text{ if } R \leq 1\\ 0 \text{ if } R > 1\end{cases},\right.$$
$$\left.\rho'(\mathbf{r}),\begin{cases}\rho'(\mathbf{r})(1-R)^{1/2} \text{ if } R \leq 1\\ 0 \text{ if } R > 1\end{cases}\right) \tag{8}$$

where $E_{xc}(\rho,m,\rho',m')$ was introduced in eq 6a. The meaning of eq 8 is that we start with an exchange-correlation functional written in the form of eq 6a, and wherever m or m' appears, we substitute as in eq 8. We call this translation of a GA functional, tGA, where t denotes translated. We have tested tPBE and tBLYP in previous work.[25,26] In eq 8, only the gradient of the total density is used, and we did not include the gradient of the on-top pair density due to the discontinuity when $R > 1$.

There are two reasons to go beyond the above translation. First, we want to include the gradient of the on-top density to be able to take advantage of the physics contained in this quantity when we design new density functionals. Second, we want the functional to have continuous first and second derivatives to facilitate the later incorporation of the on-top density functional into the SCF procedure. In order to include the gradient of the on-top pair density in a continuous way, we first make a new translation that is continuous with continuous first and second derivatives. After systematic testing, we chose the following translation prescription for a fully translated gradient approximation or ftGA

$$E_{ot}^{ftGA}[\rho(\mathbf{r}),\Pi(\mathbf{r})] =$$
$$E_{xc}\left(\rho(\mathbf{r}),\begin{cases}\rho(\mathbf{r})\chi_t(R) \text{ for } R < R_0\\ \rho(\mathbf{r})\chi_{ft}(R) \text{ for } R_0 \leq R \leq R_1\\ 0 \text{ for } R > R_1\end{cases},\rho'(\mathbf{r}),\right.$$
$$\left.\begin{cases}\rho'(\mathbf{r})\chi_t(R) + \rho(\mathbf{r})\chi_t'(R) \text{ for } R < R_0\\ \rho'(\mathbf{r})\chi_{ft}(R) + \rho(\mathbf{r})\chi_{ft}'(R) \text{ for } R_0 \leq R \leq R_1\\ 0 \text{ for } R > R_1\end{cases}\right) \tag{9}$$

where $\chi_t(R)$, $\chi_{ft}(R)$, $\chi_t'(R)$, and $\chi_{ft}'(R)$ are defined as

$$\chi_t(R) = (1-R)^{1/2}$$

$$\chi_{ft}(R) = A(R-R_1)^5 + B(R-R_1)^4 + C(R-R_1)^3$$

$$\chi_t'(R) = -\frac{1}{2}R'(1-R)^{-1/2}$$

and

$$\chi_{ft}'(R) =$$
$$R'[5A(R-R_1)^4 + 4B(R-R_1)^3 + 3C(R-R_1)^2]$$

where A, B, and C are determined such that E_{ot} is continuous with continuous first and second derivatives, and where R_0 and R_1 are unitless parameters. On the basis of a combination of smoothness and accuracy considerations in our preliminary trials, we set $R_0 = 0.9$ and $R_1 = 1.15$ The continuity conditions then yield

$$A = -475.60656009$$
$$B = -379.47331922$$
$$C = -85.38149682$$

Equation 9 has no discontinuity and utilizes the entirety of the gradient. Moreover, we can interpret this procedure as a redefinition of $\chi(R)$, namely

$$\chi(R) = \begin{cases}\chi_t(R) & \text{for } R < R_0\\ \chi_{ft}(R) & \text{for } R_0 \leq R \leq R_1\\ 0 & \text{for } R > R_1\end{cases} \tag{10a}$$

so that

$$\chi'(R) = \begin{cases}\chi_t'(R) & \text{for } R < R_0\\ \chi_{ft}'(R) & \text{for } R_0 \leq R \leq R_1\\ 0 & \text{for } R > R_1\end{cases} \tag{10b}$$

If R_0 and R_1 were equal to 1.0, then E_{ot}^{ftGA} would equal E_{ot}^{tGA}. We plot $\chi(R)$ as a function of R, eq 10a, in Figure 1.

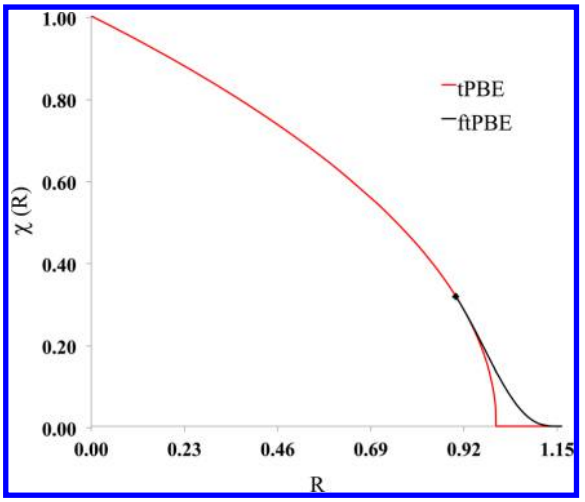

Figure 1. Plot of tPBE and ftPBE approximations to χ as a function of R. In the original translation (as used in tPBE), the red curve is followed for $0 < R \leq 1.0$, and χ is zero beyond that. In the full translation (as used in ftPBE), the red curve is followed when $0 < R < 0.9$, the black curve is followed when $0.9 \leq R \leq 1.15$, and χ is zero beyond that; this piecewise curve is continuous with continuous first and second derivatives.

DOI: 10.1021/acs.jctc.5b00609
J. Chem. Theory Comput. 2015, 11, 4077−4085

4. TEST SYSTEMS

4.1. CE56 Database and Its Subdatabases. The CE56 database was presented in an earlier article.[26] It contains 18 bond energies (6 main-group nonalkyl, 2 alkyl, and 8 transition metal), 24 diverse barrier heights, 10 diverse reaction energies, 3 proton affinities, and the complexation energy of the water dimer. Except for AgH, all data in the CE56 database are nonrelativistic electronic energies (including nuclear repulsion for molecules). For values derived from experiment, the rotational−vibrational and zero-point energies and the spin−orbit energy have been removed from experimental values as described in detail in previous work.[12] For atomization energies, we divide the atomization energy by the number of bonds in the molecule to produce the average bond energy for that molecule (thus, we call these results bond energies or atomization energies per bond; the reason for this division is so that the large atomization energies of large molecules do not have an excessive effect on the mean errors). The seven subdatabases that comprise the CE56 database are all based on previous work[9,12,30−38] and are explained in Table 1.

Table 1. Description of Types of Energetics in Each Subdatabase

subdatabase	description of elements in subdatabase
MGABE6	main-group average bond energies of six complexes. The MGABE6 is obtained from a database (AE6, from ref 32) of six atomization energies by dividing each bond energy by the number of bonds in the molecule.
TMABE10	average bond energies of 10 transition metal containing molecules: reference data for AgH and FeH from ref 9, for CoH from ref 38, and the other 7 from Zhang et al. (ref 12)
DBH24/08	diverse barrier heights for 24 representative reactions from refs 31, 32, 34, and 37 (the "/08" denotes the use of the updated 2008[34] version of the database)
DRE10	10 diverse reaction energies from the DBH24/10 subdatabase
PA3	small molecule proton affinities of three molecules taken from ref 35
ABDE2	alkyl bond dissociation energies of two molecules from refs 32, 33, and 36
WDCE1	complexation energy of a water dimer from ref 30
MGE46	combination of MGABE6, PA3, ABDE2, WDCE1, DBH24/08, and DRE10

4.2. Transition Metal Dimers and a Dinuclear Complex. We chose to study Ag_2, Cu_2, and Cr_2 because they represent some difficult cases for which accurate experimental results are available. In addition, we selected Os_2 for this study because a recent study identified it as a difficult system for KS-DFT. Finally, we study excitation energies in the $Re_2Cl_8^{2-}$ ion.

5. COMPUTATIONAL DETAILS

For the CE56 database, all MC-PDFT, CASSCF, and CASPT2 calculations were performed with a locally modified version of the *Molcas 8.1* electronic structure package.[39] All calculations for this database are nonrelativistic except when the Ag atom is present (see below). Geometries were obtained from the respective databases specified in Table 1. The basis sets used for the database containing transition metals were def2-TZVP[40] for metals and ma-TZVP[41] for other atoms. For Ag, the def2-TZVP relativistic effective core potential was used. Calculations for all databases not containing transition metals used the MG3S[42] basis set. Atomization energies are computed as the difference between the sum of the energies of the atoms and the energy of molecule.

Reasonable CASSCF active spaces were selected for each system to appropriately describe the chemistry in each case. The active spaces for the transition metal dimers are specified in footnotes to tables; active spaces used for CE56 are the same as those used previously. In all cases, we use the same active space for CASSCF, CASPT2, and MC-PDFT.

All CASPT2 calculations in this article were performed with the standard imaginary shift[43] value of 5.44 eV that serves to remediate the issue of intruder states. We also follow the usual convention of employing an IPEA shift in the zeroth order Hamiltonian of CASPT2. Except where specified otherwise (for Cr_2), we employ the *Molcas* default IPEA shift of 6.80 eV that was determined empirically[44] by considering the calculated dissociation energies of a database of 49 diatomic molecules. Note that the imaginary shift and the IPEA shift have no effect on the CASSCF or MC-PDFT results (MC-PDFT does not have the intruder state problem, and it does not require an empirical shift parameter).

In the CASPT2 calculations, we did not correlate the core orbitals. In particular, for the main group, we did not correlate 1s orbitals; for the third period, we did not correlate 1s, 2s, and 2p orbitals, except for Si, for which we did not correlate only 1s and 2s; for 3d transition metals, we did not correlate 1s, 2s, 2p, and 3s orbitals; and for Ag, we did not correlate 1s, 2s, 2p, 3s, 3p, 3d, and 4s orbitals. For Os_2, we did not correlate 1s, 2s, 2p, 3s, 3p, 3d, 4s, 4p, and 4d orbitals. For $Re_2Cl_8^{2-}$, we correlate only the 5p and 5d orbitals of Re and only the 3s and 3p orbitals of Cl.

KS-DFT results (PBE) for CE56 are presented for comparison and were obtained from previous work.[38]

For the three potential curves of transition metal dimers presented in this article, we used individually selected basis sets. For Cr_2, the cc-pVTZ-DK basis set was used.[45] For Cu_2, def2-TZVP[40] with the Douglas−Kroll−Hess (DKH) Hamiltonian[46] was used. For Ag_2, we used the def2-TZVP basis set with an effective core potential replacing 28 electrons.[40]

For calculating the equilibrium internuclear distance and excitation energy of Os_2, we used the ANO-RCC basis set with the [9s8p6d4f3g][47] contraction and with the DKH Hamiltonian. For $Re_2Cl_8^{2-}$, we used the ANO-RCC-VTZP[47,48] basis set with the DKH Hamiltonian.

6. RESULTS

We tested the new ftPBE functional using the same representative CE56 database that was used to benchmark our tPBE functional; see Table 1. The average errors are shown in Tables 2 and 3, and the complete data can be found in the Supporting Information.

Table 2. Average Mean Unsigned Errors (kcal/mol) for Entire Database and Breakdown into Subdatabase Containing Transition Metals and the Rest

	CASSCF	CASPT2	ftPBE[a]	tPBE[b]	PBE
MUE(CE56)[c]	12.4	2.7	3.3	3.2	6.9
MUE(TMABE10)[d]	22.2	5.5	3.9	4.5	7.6
MUE(MGE46)[e]	10.3	2.0	3.2	2.9	6.7

[a] $R_0 = 0.90$; $R_1 = 1.15$ in eq 6. [b] $R_0 = 1$; $R_1 = 1$ in eq 6. [c] The mean unsigned errors averaged over all data in the database. [d] The mean unsigned errors from the transition metal subdatabase. [e] The mean unsigned errors averaged over all data except those for molecules containing transition metals.

DOI: 10.1021/acs.jctc.5b00609
J. Chem. Theory Comput. 2015, 11, 4077−4085

Table 3. Average Mean Unsigned Errors (kcal/mol) for Subdatabases

	CASSCF	CASPT2	ftPBE	tPBE	PBE
MGABE6	16.5	3.8	2.2	2.3	4.4
TMABE10	22.2	5.5	3.9	4.5	7.6
DBH24/08	10.0	1.6	3.3	3.1	8.5
DRE10	8.5	2.5	4.4	4.1	6.0
PA3	5.5	0.6	1.0	0.3	1.0
ABDE2	19.1	2.6	2.5	0.5	8.3
WDCE1	0.96	0.5	1.3	0.2	0.5

After testing the stability of the ftPBE functional against the data set and finding improved performance for transition metal systems, we tested our ftPBE functional on some transition metal dimers that are a challenge for quantum chemistry, as discussed in the Introduction. The results for equilibrium geometries and dissociation energies are shown in Tables 4–6. We also show the potential energy curves in Figures 2–4.

Table 4. Silver Dimer Geometries and Dissociation Energies with the def2-TZVP Basis Set

	R_e (Å)	D_e (eV)
CASSCF[a]	2.767	0.74
CASPT2[a]	2.548	1.58
tPBE[a]	2.580	1.50
ftPBE[a]	2.575	1.64
PBE	2.574	1.77
Exp.	2.530[b]	1.65 ± 0.03[c]

[a]The active space was 2/2, corresponding to the 4s electrons and orbitals. [b]Ref 49. [c]Ref 51.

Table 5. Chromium Dimer Geometries and Dissociation Energies with the cc-pVTZ-DK Basis Set

	R_e (Å)	D_e (eV)
CASSCF[a]	3.227	0.13
CASPT2[a]	2.506	0.99*
CASPT2[a]	1.713	1.42**
tPBE[a]	1.727	0.60
ftPBE[a]	1.674	1.17
PBE	1.703	1.63
Exp.	1.680[b]	1.47[b]

[a]The active space for the CASSCF, tPBE, and ftPBE calculations is 12/12, corresponding to the 3s and 3d electrons and orbitals. For CASPT2, * denotes IPEA= 6.80 eV and ** denotes IPEA= 12.25 eV.[14] [b]Ref 13.

Table 6. Copper Dimer Geometries and Dissociation Energies with the def2-TZVP Basis Set with DKH

	R_e (Å)	D_e (eV)
CASSCF[a]	2.456	0.87
CASPT2[a]	2.246	1.86
tPBE[a]	2.258	1.85
ftPBE[a]	2.255	1.98
PBE	2.235	2.23
Exp.	2.219[b]	2.08 ± 0.02[c]

[a]The active space was 2/2, corresponding to the 3s electrons and orbitals. [b]Ref 51. [c]Ref 50.

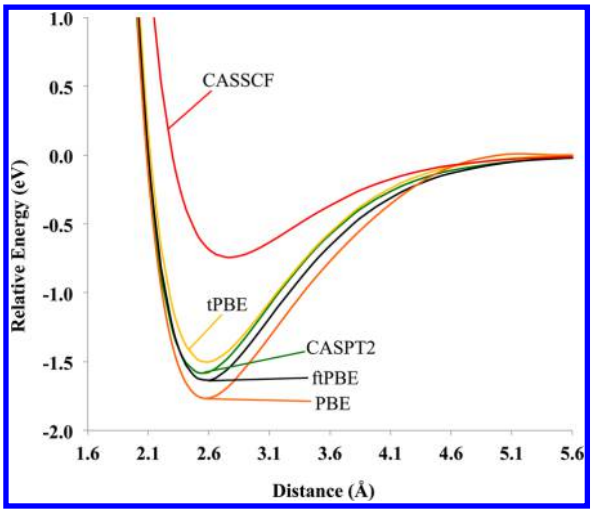

Figure 2. Silver dimer potential energy curves with def2-TZVP basis set.

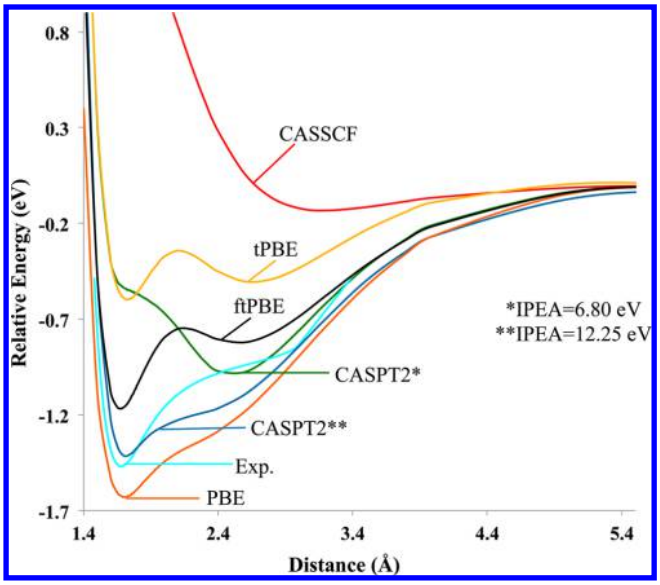

Figure 3. Chromium dimer potential energy curves with cc-pVTZ-DK basis set Cr_2.

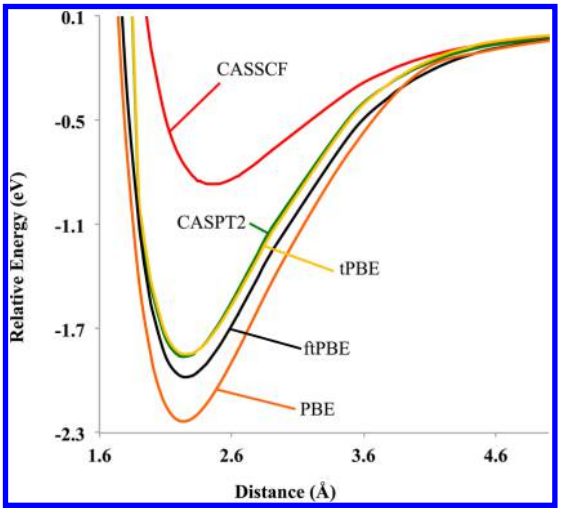

Figure 4. Copper dimer potential energy curves with def2-TZVP basis set and DKH relativistic Hamiltonian.

DOI: 10.1021/acs.jctc.5b00609
J. Chem. Theory Comput. 2015, 11, 4077–4085

7. DISCUSSION

7.1. CE56 Data Set. The overall performance of the ftPBE functional, which includes the gradient of both ρ and Π, is similar to that of tPBE for the CE56 database with a MUE of 3.2 kcal/mol, 3.2 kcal/mol for tPBE and 3.3 kcal/mol for ftPBE, as shown in Table 2. For the main-group energetics, the average errors are slightly lower for tPBE compared to those for ftPBE and the performance is still better than PBE by about a factor of 2 and worse than CASPT2 by about 1 kcal/mol. For transition metal atomization energies, ftPBE improves upon the performance of tPBE and has about 1.5 kcal/mol smaller error than CASPT2. The errors are approximately cut in half with ftPBE when compared to those with PBE. In all of the data sets, ftPBE lowers the errors relative to CASSCF, a method that is missing substantial dynamic correlation in its energies.

The performance of ftPBE for the subdatabases that make up the CE56 data set is shown in Table 3. For main-group atomization energies, ftPBE is similar to tPBE and halves the errors relative to PBE and CASPT2. For reaction barrier heights, ftPBE gives slightly higher errors by around 0.2 kcal/mol than tPBE, but it still outperforms PBE. For these types of energetics, despite the addition of the gradient of the on-top pair density, CASPT2 still outperforms ftPBE, as well as tPBE, but that performance comes at the cost of greatly increased computation time and memory. Comparing the reaction energies of the various methods, ftPBE does about the same as tPBE and falls between the performance of CASPT2 and PBE. In the case of proton affinities, the errors for ftPBE have increased relative to tPBE, but they are no worse than PBE and similar to CASPT2. Alkyl bond dissociation energies are another case where ftPBE has about doubled the errors that were found with tPBE, but they are still over a factor of 3 times smaller than those with PBE. Lastly, the energy of hydrogen bonding for a water dimer has the largest increase in errors by a factor of 6.5 for ftPBE relative to those with tPBE. Even in this case, it is no worse than CASPT2. In all cases in Table 3, ftPBE lowers the average errors relative to CASSCF.

Although the fully translated functional does not result in a decrease in the average error, we consider the incorporation of the gradient of the on-top pair density to be a success for the following reasons. First, we have now shown that the results are not sensitive to full translation of an existing GA functional. Second, we want to be able to take advantage of the gradient of the on-top density when we design improved functionals, so it is important that we have established a stable starting point for such optimization.

Finally, results presented in the Supporting Information show that ftPBE is not as sensitive to basis set as CASPT2, which is another attractive feature of this method.

7.2. Transition Metal Dimers. *7.2.1. Ag_2.* Experimentally, the silver dimer has an equilibrium bond length of 2.530 Å.[49] Most computational methods tend to overestimate the equilibrium bond length of Ag_2, and, as shown in Table 4, our results also show an elongated equilibrium geometry compared to experiment. It is well-known that CASSCF does not recover all the dynamic correlation, and post-SCF methods such as CASPT2 are necessary to account for this correlation. The ground state geometry shortens in length from 2.767 Å by CASSCF to 2.548 Å by CASPT2. The ground state geometries obtained by both MC-PDFT functionals are more similar to KS-PBE than to CASPT2, but they are within 0.05 Å of experiment. Comparing tPBE with ftPBE, i.e., adding the gradient of Π and smoothing the translation, decreases the equilibrium bond length, although only modestly.

For the dissociation energy, ftPBE is the most accurate of the methods tested in Table 4, and the improvement over tPBE is substantial. The dissociation energy increases from 0.74 eV for CASSCF to 1.64 eV for ftPBE, which shows that the effect of dynamic correlation is very large. The potential energy curves for Ag_2 are shown in Figure 1, which shows that ftPBE potential energy curve is very reasonable.

7.2.2. Cr_2. The chromium dimer is a well-known example where accounting for intrinsically multideterminantal character is essential. The potential energy curves are shown in Figure 3 for the various methods tested in this work. Experimentally, the equilibrium bond distance is 1.680 Å, with a second feature in the potential energy curve around 2.6 Å.[13] The experiments are not definitive on whether this second feature is a shoulder or a second minimum. With that being said, in the following, we will refer to it as the second minimum. The CASSCF curve does not have a minimum near the equilibrium distance, corresponding to the 3d-3d bond. In Figure 3, we show the two different CASPT2 curves, corresponding to two different values of the empirical IPEA shift, and these curves are qualitatively different. One curve, obtained with the standard empirical IPEA shift parameter of 6.80 eV that is the default in *Molcas*, has a qualitatively incorrect minimum around 2.5 Å. For Cr_2, Ruipérez et al. found a molecule-specific value of 12.25 eV;[14] this molecule-specific value changes the equilibrium geometry to 1.713 Å with a small shoulder between 2.5 and 2.6 Å. Using the same CASSCF reference wave function as CASPT2, ftPBE correctly describes the dissociation of Cr_2 and, unlike CASPT2, one does not encounter the problem of intruder states or the necessity of fine-tuning empirical parameters. The equilibrium bond distance for ftPBE is only 0.006 Å shorter than experiment, and there is a small minimum around 2.6 Å. Compared to tPBE, which has two minima of approximately equal depth, the ground state geometry is shortened by adding the gradient of Π and smoothing the translation in the functional. The shape of the PBE curve is qualitatively correct but has an elongated equilibrium geometry.

The experimental dissociation energy of Cr_2 is 1.47 eV. As with Ag_2, PBE overestimates the dissociation energy, in this case by 0.16 eV. For CASPT2 with the default IPEA value of 6.80 eV, the dissociation energy is 0.99 eV, but the potential energy curve has the wrong shape. For CASPT2 with an IPEA value of 12.25 eV, the dissociation energy is 1.42 eV. The effect of adding the gradient of Π and having a smooth translation in the functional is shown clearly by the ftPBE potential energy curve. The shape of the ftPBE potential energy curve approaches experiment, and the dissociation energy is nearly double that of tPBE.

7.2.3. Cu_2. Experimentally, the copper dimer has an equilibrium bond length of 2.219 Å.[50] As for Ag_2, the tendency of theoretical methods is to overestimate the equilibrium bond length. In Table 6, all methods tested overestimate the equilibrium geometry, with PBE being the closest to experiment. Both tPBE and ftPBE shorten the geometry compared to CASSCF by about 0.2 Å, but both are longer than CASPT2 and PBE. For ftPBE, there is a slight decrease of bond length compared to tPBE.

The potential energy curves for the copper dimer are shown in Figure 4. PBE overestimates the dissociation energy by 0.15 eV, and CASSCF substantially underestimates it, by about 1.1 eV. The CASPT2 and tPBE curves are similar in shape and have dissociation energies of 1.86 and 1.85 eV, respectively. Similarly to the other two dimers, adding the gradient of Π and having a

DOI: 10.1021/acs.jctc.5b00609
J. Chem. Theory Comput. 2015, 11, 4077−4085

smooth translation in the functional results in an increase in the dissociation energy for ftPBE. Compared to experiment, the ftPBE dissociation energy is 0.1 eV below the measured dissociation energy.

7.2.4. Os_2. Compared to other transition metal dimers, there are fewer theoretical studies on Os_2. Due to its multiconfigurational character, the predictions depend strongly on the choice of functional and basis set, with the calculated ground state being either $^7\Delta_u$ or a $^5\Pi_u$.[52−55] In addition to a KS-DFT study, Kim et al.[55] reported CASSCF, CASPT2, MRMP2, and MRCI wave function results for Os_2, and they predicted that the ground state is the $^5\Pi_u$ state. In Table 7, we report our calculated values for the dissociation energy and equilibrium geometry of Os_2, and in Table 8, we compare the energetics of the $^7\Delta_u$ and $^5\Pi_u$ states. To compare the experimental ground state dissociation energy, D_0, we subtracted the zero-point vibrational energy, which was calculated to be 0.02 eV by using the VIBROT module in *Molcas*. The resulting D_0 values are in Table 7.

Table 7. Osmium Dimer Geometries and Dissociation Energies of the $^5\Pi_u$ state

	R_e (Å)	D_0 (eV)
CASSCF[a]	2.163	1.36
CASPT2[a]	2.103	4.56
tPBE[a]	2.122	4.33
ftPBE[a]	2.121	4.25
PBE[b]	2.122	4.64
Exp.	N/A	4.3 ± 0.8[c]

[a]The active space was 16/12, corresponding to the 5d and 6s electrons and orbitals. The basis set is ANO-RCC [9s8p6d4f3g], and scalar relativistic effects are included by the DKH method. [b]For Os_2, PBE results were obtained with the def2-TZVP basis set and a scalar-relativistic ECP. [c]Ref 56.

Table 8. Osmium Dimer Geometries and Relative Energies of the $^7\Delta_u$ and $^5\Pi_u$ States

	R_e (Å)	ΔE[a] (eV)
CASSCF[b]	2.306	0.25
CASPT2[b]	2.202	0.24
tPBE[b]	2.231	0.35
ftPBE[b]	2.235	0.37
PBE[c]	2.245	0.18

[a]$\Delta E = E(^7\Delta_u) - E(^5\Pi_u)$. [b]The active space was 16/12, corresponding to the 5d and 6s electrons and orbitals. The basis set is RCC [9s8p6d4f3g], and the DKH treatment of scalar relativistic effects is used. [c]For Os_2, PBE results are obtained with the def2-TZVP basis set and a scalar-relativistic ECP.

Table 8 shows that both tPBE and ftPBE predict a $^5\Pi_u$ ground state. While there is a large range of experimental values for the dissociation energy, many of the functionals tested by Kim and Kim[55] predict a dissociation energy (in a range of 1.83−5.47 eV) that does not fall with within the experimental range. The underestimation of many functionals is because, in part, they predict the $^7\Delta_u$ state as the ground state. The high-level MRCI +Q/dhf-QVPP and MRMP2/def2-QZVPP also (apparently incorrectly) predict a septet ground state, by 0.36 and 0.17 eV, respectively, and the calculated dissociation energies of these methods are 3.29 and 4.51 eV, respectively.[55] Considering the difficulty of the problem (the wide range of previous results) and the uncertainty in the experimental results, the tPBE and ftPBE results are both considered to be satisfactory.

7.3. $Re_2Cl_8^{2-}$. The $Re_2Cl_8^{2-}$ ion, like Cr_2, presents an example of metal−metal multiple bonding. The CASSCF calculations yield a significantly multiconfigurational $^1A_{1g}$ ground state (the weights of the two most important configurations are 66 and 15%) that has natural orbital occupation numbers of 1.54 and 0.46 in the δ and δ^* orbitals, respectively.[57] The lowest-energy excitation is an intra-d-band transition, in particular, a δ to δ^* transition ($^1A_{1g}$ to $^1A_{2u}$). The excited state is also significantly multiconfigurational (the weight of the dominant configuration is 74%); it is an open-shell singlet and is a good test case for MC-PDFT. The excitations in this ion were examined with CASPT2,[57] and those calculations reproduced the experimental electronic spectrum well.[58]

The excitation energies are shown in Table 9, calculated using the experimental geometry of Cotton et al.[59] With CASPT2, the $^1A_{1g}$ to $^1A_{2u}$ excitation energy is 2.03 eV compared to the experimental value of 1.82 eV.[58] PBE underestimates the excitation energy by 1.1 eV, and tPBE and ftPBE underestimate it by 0.6−0.8 eV, which is not useful accuracy. As usual for comparing the energies of states of different symmetry, the results in Table 9 correspond to carrying out separate CASSCF and CASPT2 calculations for each symmetry. Curiously, if we use the ground state orbitals for both states (i.e., treat the excited state by CASCI with ground state orbitals), then the calculated excitation energies increase to 2.02 eV for tPBE and 1.89 eV for ftPBE, in better agreement with experiment but probably fortuitously. The sensitivity of the results to the way the orbitals are optimized will be an interesting subject for further study.

Table 9. $Re_2Cl_8^{2-}$ Excitation Energies for the δ to δ^* Transition ($^1A_{1g}$ to $^1A_{2u}$) with the ANO-RCC-VTZP Basis Set with DKH

	ΔE (eV)
CASSCF[a]	3.08
CASPT2[a]	2.03
tPBE[a]	1.18
ftPBE[a]	1.03
PBE[b]	0.69
Exp.[c]	1.82 ± 0.02

[a]The active space was 12/12 corresponding to eight Re−Re 5d bonding/antibonding orbitals and four Re−Cl bonding/antibonding orbitals. [b]ΔSCF energies. [c]Ref 58.

8. CONCLUSIONS

We have presented a full-translation prescription for deriving on-top density functionals for MC-PDFT. The resulting functionals include the gradient of the on-top pair density as well as of the total one-particle density, and they have continuous first and second derivatives. We find that MC-PDFT is stable with respect to including the gradient of the on-top density. Furthermore, we find that the new ftPBE on-top density functional performs about as well as the original tPBE translation for overall energetics of the CE56 database, but it provides an improvement for system with transition metal−transition metal bonds. To examine this further, we present full potential curve calculations for Cr_2, Cu_2, and Ag_2, and these calculations show that our new ftPBE functional improves over the original tPBE functional in these cases. In the case of the transition metal dimers presented here, ftPBE has more accurate dissociation energies and bond lengths

DOI: 10.1021/acs.jctc.5b00609
J. Chem. Theory Comput. 2015, 11, 4077−4085

than tPBE and is more accurate than CASPT2 for dissociation energies. Although the bond lengths of the silver and copper dimers are elongated compared to experiment, consideration of the energetics and potential energy curves, particularly of the chromium dimer, seems to indicate that including the gradient of the on-top density accounts for important physics that is missing in the tGA translation.

We also present calculations on the difficult Os_2 system and obtain satisfactory results for both bond lengths and quintet−septet splittings; the latter appear to be more accurate than values calculated by MRCI. Finally, we present results for the $\delta \rightarrow \delta^*$ excitation of $Re_2Cl_8^{2-}$, where the method is less successful.

We hope that it will be possible to build on the present results in designing new functionals. The good accuracy obtained so far with MC-PDFT is encouraging. One can obtain results comparable in quality to CASPT2 but at much lower cost and with lower basis-set dependence, as well as having the spatial and spin symmetries of the approximated states represented explicitly and correctly. The method is very promising for treating systems that are intrinsically multideterminantal in character.

■ ASSOCIATED CONTENT

Supporting Information

The Supporting Information is available free of charge on the ACS Publications website at DOI: 10.1021/acs.jctc.5b00609.

Energetics for CE56 for CASSCF, CASPT2, tPBE, ftPBE, and PBE; energetics and geometries for Cu_2 and Ag_2 with other basis sets; Cartesian coordinates for $Re_2Cl_8^{2-}$; and constants for ftGA functional (PDF).

■ AUTHOR INFORMATION

Corresponding Authors

*(D.G.T.) E-mail: truhlar@umn.edu.

*(L.G.) E-mail: gagliardi@umn.edu.

Funding

This research was supported by the Inorganometallic Catalyst Design Center, an Energy Frontier Research Center funded by the U.S. Department of Energy, Office of Basic Energy Sciences, Division of Chemical Sciences, under award DE-SC0012702. R.K.C. thanks the National Science Foundation for a Graduate Research Fellowship under grant no. 00039202.

Notes

The authors declare no competing financial interest.

■ ACKNOWLEDGMENTS

The authors are grateful to Giovanni Li Manni, Andrew L. Sonnenberger, and Chad Hoyer for helpful assistance and to Doreen Leopold for helpful discussions.

■ REFERENCES

(1) Kohn, W.; Sham, L. J. *Phys. Rev.* **1965**, *140*, A1133−A1138.
(2) Noodleman, L. *J. Chem. Phys.* **1981**, *74*, 5737-.
(3) Yamaguchi, K.; Tsunekawa, T.; Toyoda, Y.; Fueno, T. *Chem. Phys. Lett.* **1988**, *143*, 371−376.
(4) Yamaguchi, K.; Jensen, F.; Dorigo, A.; Houk, K. N. *Chem. Phys. Lett.* **1988**, *149*, 537.
(5) Cramer, C. J.; Truhlar, D. G. *Phys. Chem. Chem. Phys.* **2009**, *11*, 10757−10816.
(6) Perdew, J. P.; Savin, A.; Burke, K. *Phys. Rev. A: At., Mol., Opt. Phys.* **1995**, *51*, 4531−4541.
(7) Ruzsinszky, A.; Perdew, J. P.; Csonka, G. I. *J. Phys. Chem. A* **2005**, *109*, 11006−11014.
(8) Hohenberg, P.; Kohn, W. *Phys. Rev.* **1964**, *136*, 864−871.
(9) Schultz, N. E.; Zhao, Y.; Truhlar, D. G. *J. Phys. Chem. A* **2005**, *109*, 11127−11143.
(10) Harvey, J. N. *Annu. Rep. Prog. Chem., Sect. C: Phys. Chem.* **2006**, *102*, 203−226.
(11) Cohen, A. J.; Mori-Sánchez, P.; Yang, W. *Science* **2008**, *321*, 792−794.
(12) Zhang, W.; Truhlar, D. G.; Tang, M. *J. Chem. Theory Comput.* **2013**, *9*, 3965−3977.
(13) Casey, S. M.; Leopold, D. G. *J. Phys. Chem.* **1993**, *97*, 816−830.
(14) Ruipérez, F.; Aquilante, F.; Ugalde, J. M.; Infante, I. *J. Chem. Theory Comput.* **2011**, *7*, 1640−1646.
(15) Roos, B. O.; Taylor, P. R.; Siegbahn, P. E. M. *Chem. Phys.* **1980**, *48*, 157−173.
(16) Andersson, K.; Malmqvist, P.-A.; Roos, B. O. *J. Chem. Phys.* **1992**, *96*, 1218−1226.
(17) Li Manni, G.; Ma, D.; Aquilante, F.; Olsen, J.; Gagliardi, L. *J. Chem. Theory Comput.* **2013**, *9*, 3375−3384.
(18) Scuseria, G. E. *J. Chem. Phys.* **1991**, *94*, 442−447.
(19) Gutsev, G. L.; Bauschlicher, C. W. *J. Phys. Chem. A* **2003**, *107*, 4755−4767.
(20) Barden, C. J.; Rienstra-Kiracofe, J. C.; Schaefer, H. F. *J. Chem. Phys.* **2000**, *113*, 690−700.
(21) Schultz, N. E.; Zhao, Y.; Truhlar, D. G. *J. Phys. Chem. A* **2005**, *109*, 4388−4403.
(22) Brynda, M.; Gagliardi, L.; Roos, B. O. *Chem. Phys. Lett.* **2009**, *471*, 1−10.
(23) Yanagisawa, S.; Tsuneda, T.; Hirao, K. *J. Chem. Phys.* **2000**, *112*, 545−553.
(24) Pou-AméRigo, R.; Merchán, M.; Nebot-Gil, I.; Malmqvist, P.-Å.; Roos, B. O. *J. Chem. Phys.* **1994**, *101*, 4893−4902.
(25) Li Manni, G.; Carlson, R. K.; Luo, S.; Ma, D.; Olsen, J.; Truhlar, D. G.; Gagliardi, L. *J. Chem. Theory Comput.* **2014**, *10*, 3669−3680.
(26) Carlson, R. K.; Li Manni, G.; Sonnenberger, A. L.; Truhlar, D. G.; Gagliardi, L. *J. Chem. Theory Comput.* **2015**, *11*, 82−90.
(27) (a) Colle, R.; Salvetti, O. *Theor. Chim. Acta* **1975**, *37*, 329-. (b) Colle, R.; Salvetti, O. *Theor. Chim. Acta* **1979**, *53*, 55-. (c) Moscardó, F.; San-Fabián, E. *Phys. Rev. A: At., Mol., Opt. Phys.* **1991**, *44*, 1549-. (d) Miehlich, B.; Stoll, H.; Savin, A. *Mol. Phys.* **1997**, *91*, 527-. (e) Gräfenstein, J.; Cremer, D. *Chem. Phys. Lett.* **2000**, *316*, 569-. (f) Gräfenstein, J.; Cremer, D. *Phys. Chem. Chem. Phys.* **2000**, *2*, 2091-. (g) McDouall, J. J. W. *Mol. Phys.* **2003**, *101*, 361-. (h) Takeda, R.; Yamanaka, S.; Yamaguchi, K. *Int. J. Quantum Chem.* **2004**, *96*, 463-. (i) Gusarov, S.; Malmqvist, P.-A.; Lindh, R. *Mol. Phys.* **2004**, *102*, 2207. (j) Gräfenstein, J.; Cremer, D. *Mol. Phys.* **2005**, *103*, 279. (k) Pérez-Jiménez, Á. J.; Pérez-Jordá, J. M.; Sancho-García, J. C. *J. Chem. Phys.* **2007**, *127*, 104102.
(28) Perdew, J. P.; Burke, K.; Ernzerhof, M. *Phys. Rev. Lett.* **1996**, *77*, 3865−3868.
(29) Becke, A. D.; Savin, A.; Stoll, H. *Theor. Chim. Acta* **1995**, *91*, 147−156.
(30) Zhao, Y.; Truhlar, D. G. *J. Chem. Theory Comput.* **2005**, *1*, 415−432.
(31) Zhao, Y.; González-Garcia, N.; Truhlar, D. G. *J. Phys. Chem. A* **2005**, *109*, 2012−2018.
(32) Zhao, Y.; Schultz, N. E.; Truhlar, D. G. *J. Chem. Theory Comput.* **2006**, *2*, 364−382.
(33) Izgorodina, E. I.; Coote, M. L.; Radom, L. *J. Phys. Chem. A* **2005**, *109*, 7558−7566.
(34) Zheng, J.; Zhao, Y.; Truhlar, D. G. *J. Chem. Theory Comput.* **2009**, *5*, 808−821.
(35) Zhao, Y.; Truhlar, D. G. *J. Phys. Chem. A* **2006**, *110*, 10478−10486.
(36) Zhao, Y.; Truhlar, D. G. *J. Chem. Phys.* **2006**, *125*, 194101.
(37) Zhao, Y.; Lynch, B. J.; Truhlar, D. G. *Phys. Chem. Chem. Phys.* **2005**, *7*, 43−52.
(38) Peverati, R.; Truhlar, D. G. *Philos. Trans. R. Soc., A* **2014**, *372*, 20120476.
(39) Aquilante, F.; De Vico, L.; Ferré, N.; Ghigo, G.; Malmqvist, P.-Å; Neogrády, P.; Pedersen, T. B.; Pitonak, M.; Reiher, M.; Roos, B. O.;

DOI: 10.1021/acs.jctc.5b00609
J. Chem. Theory Comput. 2015, 11, 4077−4085

Serrano-Andrés, L.; Urban, M.; Veryazov, V.; Lindh, R. *J. Comput. Chem.* **2010**, *31*, 224−247.
(40) Weigend, F.; Ahlrichs, R. *Phys. Chem. Chem. Phys.* **2005**, *7*, 3297−3305.
(41) Zheng, J.; Xu, X.; Truhlar, D. G. *Theor. Chem. Acc.* **2011**, *128*, 295−305.
(42) Lynch, B. J.; Zhao, Y.; Truhlar, D. G. *J. Phys. Chem. A* **2003**, *107*, 1384−1388.
(43) Forsberg, N.; Malmqvist, P.-Å. *Chem. Phys. Lett.* **1997**, *274*, 196−204.
(44) Ghigo, G.; Roos, B. O.; Malmqvist, P. Å. *Chem. Phys. Lett.* **2004**, *396*, 142−149.
(45) Balabanov, N. B.; Peterson, K. A. *J. Chem. Phys.* **2005**, *123*, 064107.
(46) Reiher, M. *Wiley Interdiscip. Rev. Comput. Mol. Sci.* **2012**, *2*, 139−149.
(47) Roos, B. O.; Lindh, R.; Malmqvist, P.-Å.; Veryazov, V.; Widmark, P.-O. *J. Phys. Chem. A* **2005**, *109*, 6575−6579.
(48) Roos, B. O.; Lindh, R.; Malmqvist, P.-Å.; Veryazov, V.; Widmark, P.-O. *J. Phys. Chem. A* **2004**, *108*, 2851−2858.
(49) Simard, B.; Hackett, P. A.; James, A. M.; Langridge-Smith, P. R. R. *Chem. Phys. Lett.* **1991**, *186*, 415−422.
(50) Rohlfing, E. A.; Valentini, J. J. *J. Chem. Phys.* **1986**, *84*, 6560−6566.
(51) Lombardi, J. R.; Davis, B. *Chem. Rev.* **2002**, *102*, 2431−2460.
(52) Wu, Z. J.; Han, B.; Dai, Z. W.; Jin, P. C. *Chem. Phys. Lett.* **2005**, *403*, 367.
(53) Du, J. G.; Sun, X. Y.; Wang, H. Y. *Int. J. Quantum Chem.* **2008**, *108*, 1505.
(54) Takahashi, K.; Isobe, S.; Ohnuki, S. *Chem. Phys. Lett.* **2013**, *555*, 26−30.
(55) Kim, J.; Kim, J. *Int. J. Quantum Chem.* **2014**, *114*, 1466−1471.
(56) Morse, M. D. *Chem. Rev.* **1986**, *86*, 1049−1109.
(57) Gagliardi, L.; Roos, B. O. *Inorg. Chem.* **2003**, *42*, 1599−1603.
(58) Trogler, W. C.; Gray, H. B. *Acc. Chem. Res.* **1978**, *11*, 232−239.
(59) Cotton, F. A.; Harris, C. B. *Inorg. Chem.* **1965**, *4*, 330.

DOI: 10.1021/acs.jctc.5b00609
J. Chem. Theory Comput. 2015, 11, 4077−4085